ELSEVIER

Turbulent flow and heat transfer measurements on a curved surface with a fully developed round impinging jet

D. H. Lee,* Y. S. Chung,* and D. S. Kim†

*Department of Mechanical Engineering, Inje University, Kimhae, Kyungnam, South Korea, and
†Research Institute of Mechanical Technology, Pusan National University, Pusan, South Korea

The effects of the convex surface curvature on the local heat transfer from an axisymmetric impinging jet were investigated. The flow at the nozzle exit has a fully developed velocity profile. The jet Reynolds number (Re) ranges from 11,000 to 50,000, the dimensionless nozzle-to-surface distance (L/d) from 2 to 10, and the dimensionless surface curvature (d/D) from 0.034 to 0.089. The results show that the stagnation point Nusselt number (Nu_{st}) increases with increasing value of d/D. The maximum Nusselt number at the stagnation point occurs at $L/d \cong 6$ to 8 for all Res and d/Ds tested. Both the stagnation point and the average Nusselt number over the curved surface are well correlated with Re, L/d, and d/D. For larger L/d, Nu_{st} dependency on Re is stronger because of an increase of turbulence in the approaching jet as a result of the more active exchange of momentum with a surrounding air. The local Nusselt number decreases monotonically from its maximum value at the stagnation point. However, for $L/d=2$ and Re=23,000, and for $L/d \leq 4$ and Re=50,000, the streamwise Nusselt number distributions exhibit secondary maxima at $r/d \cong 2.2$.

Keywords: impinging jet; heat transfer on the curved surface; liquid crystal; uniform heat flux boundary condition

Introduction

Numerous studies of the heat transfer and flow characteristics for jet impingement on surfaces have been reported. These studies have dealt with the effects of the Reynolds number, nozzle-to-surface distance, nozzle geometry, jet temperature, orientation, multiple jets, cross flow, and impinging surface shape on the resulting flow and heat transfer. Critical reviews of impinging jet heat transfer studies have been published by Martin (1977), Jambunathan et al. (1992), and Viskanta (1993). Heat transfer measurements for various nozzle geometries and flow conditions have been made by many researchers.

Works by Gardon and co-workers (Gardon and Cobonpue 1962; Gardon and Akfirat (1965; 1966) investigated the local heat transfer coefficients for axisymmetric and planner, single or arrays of jets by using a very sensitive heat flux meter (Gardon or thin circular foil meter). Hoogendoorn (1977) studied the effect of turbulence on the heat transfer at the stagnation point with long straight pipe and smoothly convergent nozzle. Goldstein and Franchett (1988) studied heat transfer to a jet impinging at different oblique angles to a plane surface. Baughn and Shimizu (1989) and Yan (1993) have carried out heat transfer measurements with a fully developed round jet impinging on the flat surface. More recently, Lee et al. (1994; 1995) have studied the heat transfer characteristics with an air jet issuing from an elliptical nozzle and from a long straight pipe nozzle, respectively. All of the studies referenced above have investigated the heat transfer and flow characteristics for jets impinging on the flat surface. However, many industrial applications of jet impingement cooling on the curved surface may be encountered.

A few papers have studied the impinging heat transfer from the curved surface. Chupp et al. (1969) studied the local and average heat transfer with an array of round jets impinging on a concave surface. Thomann (1968) investigated the wall curvature effect on the turbulent heat transfer and found that heat transfer on the concave surface is around 20% higher than that on the flat surface. Hrycak (1981; 1982) reported the total heat transfer at the stagnation point on the concave surface is higher than for the flat surface geometry due to a larger surface area, especially for small nozzle-to-surface distances. Gau and Chung (1991) studied the effect of surface curvature on slot jet impingement heat transfer along semicylindrical concave and convex surfaces. They reported that at the stagnation point of the convex surface, the momentum transport in the flow is increased due to a series of three-dimensional (3-D) counterrotating vortices initiated near the wall, and subsequently the heat transfer rate is augmented. In the wall jet region, the flow is stabilized because of the centrifugal force, resulting in a decrease in the heat transfer rate. They also found that on a concave surface, the heat transfer rate on and around the stagnation point increases with increasing surface curvature because of an earlier initiation of vortices in the mixing region of a wider jet, which causes an earlier termination of the potential core and the enhancement in the momen-

Address reprint requests to Dr. D. H. Lee, Department of Mechanical Engineering, Inje University, 607 Obang-Dong, Kimhae, Kyungnam 621-749, South Korea.

Received 10 March 1996; accepted 15 October 1996

Int. J. Heat and Fluid Flow 18: 160–169, 1997

655 Avenue of the Americas, New York, NY 10010

0142-727X/97/$17.00
PII S0142-727X(96)00136-4

tum and energy transport along the wall. Yang et al. (1995) investigated jet impingement cooling on the semicircular concave surface with two different nozzles (round-edges nozzle and rectangular-edged nozzle). They also studied characteristics of free jets issuing from two nozzles.

In the present study, the local heat transfer coefficients are measured for an air jet issuing from a long straight pipe and impinging perpendicularly on a hemispherically convex surface. The experiments are made for Re = 11,000–50,000, $L/d = 2$–10, and $d/D = 0.034$–0.089. An electrically heated gold film Intrex (a thin gold-coated polyester sheet) is used to create a uniform heat flux on the surface. The temperature on the surface is determined using a thermochromic liquid crystal and a color image processing system as a means of the quantitative color determination on the liquid crystal.

Experimental apparatus

A diagram of the apparatus used in the experiment is shown in Figure 1. Laboratory air, delivered by a 2 h.p. centrifugal blower, first enters a 6.35-cm i.d. copper pipe that contains a cross-flow heat exchanger with water from a constant temperature bath circulating inside the heat exchanger. Then, the copper pipe connects to a 6.3-cm i.d. cast acrylic pipe in which an ASME orifice flow meter is installed. Located 150 cm downstream end of this pipe is a smooth transition into the smaller cast acrylic pipe with three inner diameters of $d = 1.3$, 2.15, and 3.4 cm and three lengths of $L = 76$, 125, and 197 cm. Therefore, a fully developed round jet resulting from the development length-to-pipe diameter ratio of 58 impinges perpendicularly upon a convex hemispherical surface.

The jet temperature is measured by 0.025-cm chromel-alumel thermocouple inserted through a hole in the pipe 10-cm upstream from the pipe. Three thermocouples of the same type and gauge are used to measure the ambient temperature. These thermocouples are then connected to the data-acquisition system (STRAWBERRY TREE/DATAshuttle-12 and IBM-486/PC) and calibrated against a PRT (platinum resistance thermometer) in the constant temperature bath (NESLAB/RTE-221D) to within ± 0.1 °C accuracy. The pipe system is in the piston-cylinder type that permits the nozzle-to-surface distance to be changed a maximum value of $L = 40$ cm with an accuracy of 0.5 mm.

A heat exchanger is used to adjust the air temperature so that the jet issuing from the nozzle is maintained to within ± 0.2 °C of the ambient temperature. The fan speed is controlled by an inverter, and the corresponding flow rate is measured with an ASME orifice and micromanometer (MERIAM/34MB2-TM) that has an accuracy of 0.001 cm water.

The test model consists of a 1.25-mm thick and 38.1-cm diameter Plexiglas convex hemisphere to which three 60-cm long strips (one 2.5-cm wide strip in the middle as a main heater and two 1.5-cm wide strips on both sides as guard heaters) of the gold-coated Intrex is attached. The Intrex consists of a 0.13-mm thick transparent polyester film on which an approximately 20 angstroms thick of gold coating is applied by means of vacuum deposition. Copper foil strip "electrodes" are attached to both

Notation

A	surface area of the gold film Intrex
C_p	wall pressure coefficient $[= P_w - P_\infty)/(0.5\rho U_{ce}^2)]$
d	pipe nozzle diameter
D	outer diameter of the hemisphere
d/D	surface curvature
D_{AB}	binary diffusion coefficient
f	gold-coating uniformity factor
I	current across the gold film Intrex
k	thermal conductivity of air
L	nozzle-to-surface distance
L/d	dimensionless nozzle-to-surface distance
Nu	local Nusselt number $(= hd/k)$
Nu_{ave}	average Nusselt number over the curved surface
Nu_{st}	stagnation point Nusselt number
P_w	wall pressure on the hemisphere surface
P_∞	atmospheric pressure
q_c	conduction heat loss
q_v	net heat flux
r	streamwise distance from the stagnation point
r/d	dimensionless streamwise distance from the stagnation point
R	radius of the pipe nozzle
Re	Reynolds number based on mean velocity and nozzle diameter $(= Ud/\nu)$
Re_{max}	Reynolds number based on maximum velocity $(= U_{max}\, d/\nu)$
Sc	Schmidt number, $(= \nu/D_{AB})$
T_a	ambient temperature
T_j	jet temperature
T_W	wall temperature of the convex surface
u	fluctuating velocity in the axial direction on the jet centerline
U_c	jet centerline mean velocity
U_{ce}	jet centerline mean velocity at the nozzle exit
$\sqrt{\overline{u^2}}/U_{ce}$	turbulent intensity at the nozzle exit
U_{max}	maximum mean velocity inside the nozzle
V	voltage across the gold film Intrex
y	radial position measured from the pipe wall

Greek

ε	emissivity of the liquid crystal and black paint coated surface (measured by infrared radiation thermometer: Minolta/505S)
ν	kinematic viscosity of air
ρ	density of air
σ	Stefan–Boltzmann constant

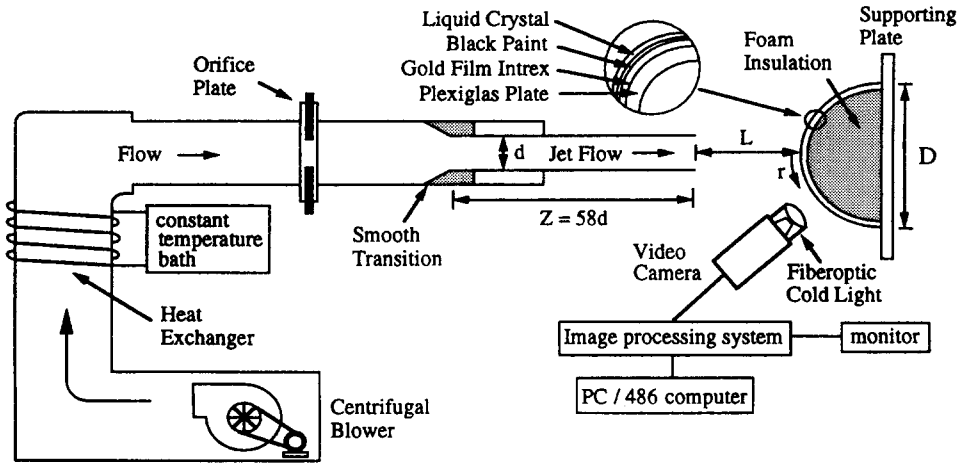

Figure 1 Schematic diagram of the test apparatus for the jet impingement on the curved surface

ends of the Intrex strip surfaces and silver-loaded paint is applied to establish a good electrical contact between the copper electrodes and the strip surfaces. The copper electrodes are connected to an adjustable dc power supplier in series with a current shunt (rated 50 mV and 5 amps), allowing an adjustable voltage to be supplied to the electrodes and the voltage drop across and current input to the Intrex to be measured. Two Fluke 8842A Multimeters with a precision to 0.1 μV are used to measure the voltages across the Intrex and current shunt. By passing dc current through a uniformly coated gold on the Intrex, an essentially uniform heat flux boundary condition is created.

The Intrex strip surface is air-brushed with a thin layer of black backing paint and liquid crystal. The liquid crystal used in this experiment is HALLCREST "R35C1W" microencapsulated thermochromic liquid crystal. It has a narrow band of approximately 1 °C over which the entire color spectrum occurs (the color red nominally starting at 35 °C and the color blue starting at 36 °C). As a last step after all these processes, to smooth out the edge created between the liquid crystal coated Intrex strips, the entire hemisphere is covered with an extremely thin flexible Mylar sheet.

To minimize the conduction heat loss and radiative heat gain, care is taken; the other side of the test section was tightly packed with urethane foam insulation and a fiber-optic cold light source was used to illuminate the liquid crystal surface. The test section is then mounted against the vertical plane and perpendicular to the direction of the jet flow. Because the actual color image is affected by such factors as the thickness of liquid crystal, the angle and distance of the light illuminating the liquid crystal coated surface, a careful color calibration was carried out under the particular conditions mentioned above and later the experiments were carried out under the same conditions as those for the calibration. To determine the particular color quantitatively and to minimize a visual bias, a digital color image processing system was used. It consisted of a color video camera (SAMSUNG/SV-F12), a color frame grabber (DARIM/Video-Catcher), and IBM-PC/486.

To ensure that the flow just before the pipe exist has a fully developed velocity profile, the mean velocity distribution for $Re_{max} = 50{,}000$ (Re = 42,000) was measured inside the 3.4-cm diameter pipe. The jet centerline velocity and turbulent intensity for Re = 11,000, 23,000 and 50,000 were also measured with/without the impinging convex surface being present. These measurements were made using TSI IFA-100 Constant Temperature Anemometer (CTA) with a TSI-1210 single straight hot-wire probe. The hot-wire output signals were low-pass filtered at 5 kHz through a TSI-1057 signal conditioner, then digitized by a universal waveform analyzer (Data Precision-D6000) that has a 14-bit A/D converter with a sampling frequency of 10 kHz. A total of 20 ensembles of 4,096 datasets were averaged and stored in a hard disk of a personal computer (IBM-PC/486). During the experiment, the ambient temperature compensation was made to the hot-wire signals. The hot-wire probe was calibrated before and after the experiment using a TSI-1125 calibrator.

To measure the wall pressure, 25 stainless steel tubes with 1-mm diameter were imbedded vertically on the curved surface. To prevent the pressure taps from interfering with one another, they were located spirally from the geometric center with a separation distance from the center increasing and with each tap 90° apart (i.e., 1 cm from tap #1 at the center to #2, 2 cm to #3, 3 cm to #4 etc.) The average pressure at a 10-s period was measured using a digital micromanometer (Furness FC012), and the ambient temperature compensation was made to minimize the uncertainty.

Data reduction

The measurement technique in this study, described by Lee et al. (1995) provides a method for determining the surface isotherm using liquid crystal. By electrically heating a very thin gold coating on the Intrex, an essentially uniform wall heat flux condition is established. The heat flux can be adjusted by changing the current through the Intrex, which changes the surface temperature. Under the constant heat flux condition, an isotherm on the Intrex surface corresponds to a contour of a constant heat transfer coefficient. As the heat flux changes, the position of the color isotherm is also moved. The local heat transfer coefficient at the position of the particular color being observed is calculated from

$$h = q_v/(T_w - T_j) \tag{1}$$

where, T_w is the wall temperature determined by liquid crystal, T_j is the jet temperature, and q_v is the net heat flux, which is obtained by subtracting the heat losses from the total heat flux on the Intrex; i.e.,

$$q_v = fIV/A - \varepsilon\sigma(T_w^4 - T_a^4) - q_c \tag{2}$$

The ratio of the local electrical heating to the average heating f is a measure of the uniformity of the gold coating. Baughn et al. (1989) found the uniformity to be as high as 98% when the test section of Intrex is small and selected from the middle of a roll where the gold-coating is most uniform, which has been the case of the present experiment. Therefore, we assume $f \approx 1$ for the heat flux calculation, but f is maintained in Equation 2, because it contributes to the overall uncertainty (see Table 1). The conduction loss q_c through the back of the plate is small compared to the surface heating and is assumed to be zero. However, it is included in the equation, because it contributes to the overall uncertainty.

The uncertainty analysis has been carried out using the method by Kline and McKlintock (1953). It is shown in Table 1 that the uncertainty in the Nusselt number for $d/D = 0.034$, $L/d = 10$, and $r/d = 5.54$ at Re = 11,000 is 4.0%. The uncertainty in the gold coating uniformity is the largest contribution to the uncertainty. Another important source of uncertainty is the emissivity of liquid crystal and black paint.

Discussion of results

Mean velocity, turbulent intensity, and wall pressure coefficient

In Figure 2, the mean velocity profile at the pipe nozzle exit for Re = 42,000 (Re_{max} = 50,000) is compared to the fully developed mean velocity profile by Laufer (1954) for Re_{max} = 50,000 (based on maximum mean velocity at the nozzle exit). It can be seen that the present velocity profile is in excellent agreement with Laufer's, because the maximum difference between the two results is only 4%. In addition, the profiles were measured across the full diameter of the pipe and were found to be symmetrical from top to bottom. Based on this comparison, although comparison was made for Re = 42,000 (Re_{max} = 50,000), the jet flow at the nozzle exit can be considered to have a fully developed velocity profile for all Reynolds numbers used in the present experiment.

Figures 3 and 4 show the profiles of the free jet centerline velocity and turbulent intensity (referenced to the free jet centerline velocity at the nozzle exit) for Re = 11,000, 23,000, and 50,000 for $d/D = 0.056$. Giralt et al. (1977) defined the potential core of the free jet to be the distance from the nozzle exit to a point where the centerline velocity U_c is 98% of the velocity at the nozzle exit U_{ce}. Using this definition, it is derived from Figure 3 that the potential core lengths are 3.1, 3.7, and 4.2 nozzle diameters from the nozzle exit for Re = 11,000, 23,000, and 50,000, respectively (i.e., longer potential core length for higher Re). Beyond the potential core, the free jet centerline velocity rapidly decays and for $L > 8d$ it decreases with the inverse of

Table 1 Nusselt number uncertainty analysis

x_i	Value	δx_i	$\left(\frac{\delta x_i}{Nu}\frac{\partial Nu}{\partial x_i}\right) \times 100$ (%)
f	1.0	0.02	2.62
ε	0.9	0.05	2.0
q_c	0 (W/m^2)	4.58	1.26
T_w	35.7, °C	0.20	1.15
T_j	13.0, °C	0.15	0.86
A	0.166, m^2	8.3×10^{-5}	0.66
I	0.183, A	7.77×10^{-4}	0.56
d	13, mm	0.05	0.46
V	41.6, V	0.125	0.39
Total Nu uncertainty: $\delta Nu/Nu = 4.0\%$			

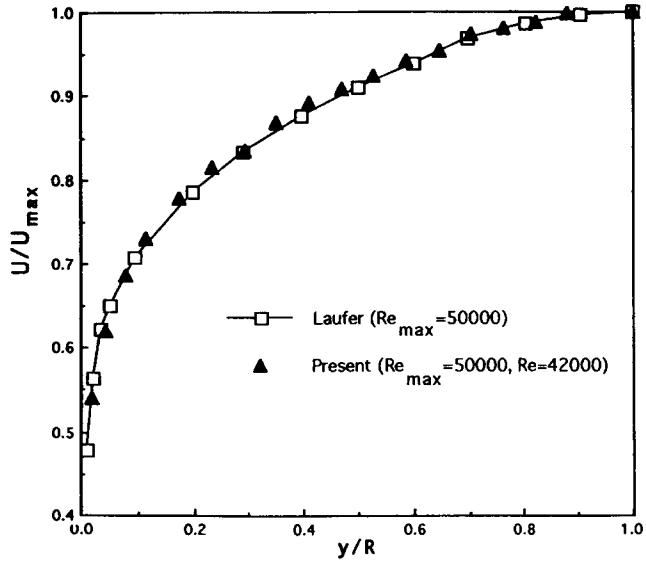

Figure 2 Mean velocity profiles (normalized by maximum velocity) at the nozzle exit

distance. The velocity profiles in three zones are well approximated as follows:

For Re = 11,000,

$$U_C/U_{ce} = 1.0 - 0.0057(L/d); \quad L/d < 3.5$$

$$U_c/U_{ce} = 1.04 - 0.044(L/d); \quad 3.5 \le L/d \le 8$$

and

$$U_c/U_{ce} = 6.9/(1.7 + L/d); \quad 8 < L/d$$

For Re = 23,000 and 50,000,

$$U_c/U_{ce} = 10 - 0.0047(L/d); \quad L/d < 5$$

$$U_c/U_{ce} = 1.26 - 0.058(L/d); \quad 5 \le L/d \le 8$$

and

$$U_c/U_{ce} = 7.45/(1.33 + L/d); \quad 8 < L/d$$

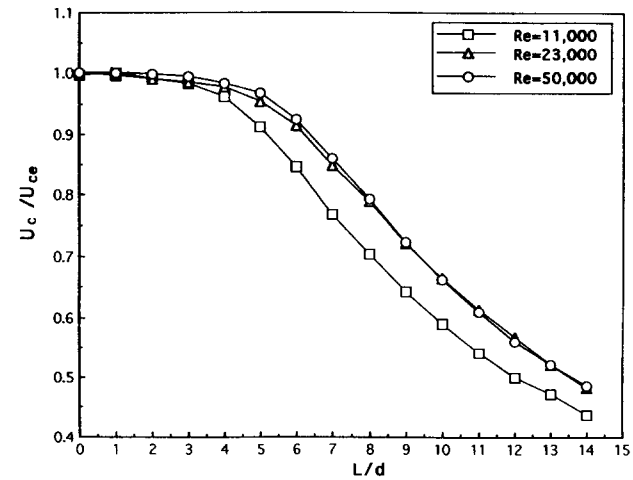

Figure 3 Mean velocity profiles along the free-jet centerline for $d/D = 0.056$.

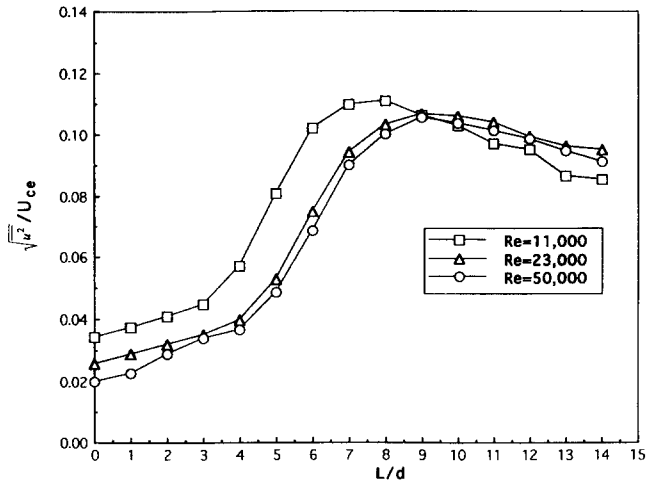

Figure 4 Turbulent intensity profiles along the free-jet centerline for $d/D=0.056$

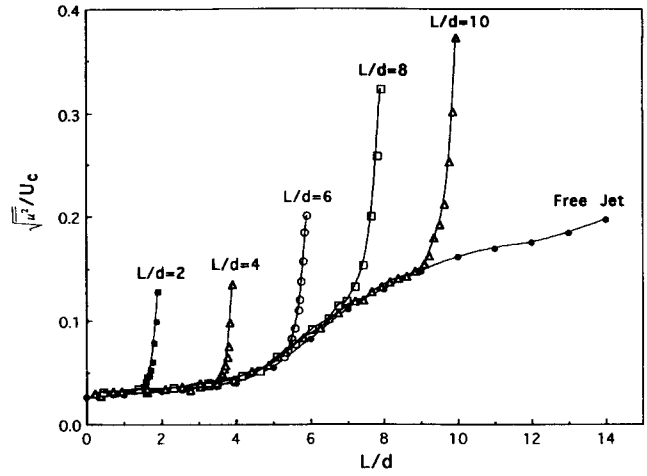

Figure 6 Free- and impinging-jet centerline furbulent intensity profiles for Re=23,000 and $d/D=0.056$

in good agreement with data by Boguslawski and Popiel (1979) for a fully developed free jet, which show the jet potential core extending for approximately 3.6 nozzle diameters for Re = 41,000.

It is observed from Figure 4 that the turbulent intensity remains roughly the same at the level of 3% in the potential core region. Beyond the potential core region, the turbulent intensity rapidly increases because of an increase of the surrounding air entrainment. After the point of $L/d \cong 8$ where the jet becomes fully developed, the turbulent intensity slowly decays. This behaviour is in good agreement with previous results by Boguslawski and Popiel (1979) and Giralt et al. (1977).

Superimposed on the free jet data given in Figures 3 and 4 for Re = 23,000 and $d/D = 0.056$, Figures 5 and 6 present the centerline velocity and turbulent intensity (referenced to the jet centerline mean velocity U_c) in the impinging jet situation as the jet approaches the convex surface for five nozzle-to-surface distances. Figure 5 shows the the impinging jet centerline velocity profiles coincide with the free jet velocity profile down to the region (i.e., the beginning of the impingement region) approximately 1.3 diameters above the surface and drastically decay afterward as the jet approaches close to the surface, which agrees with flat surface results by Giralt et al. (1977) and Rajaratnam (1976).

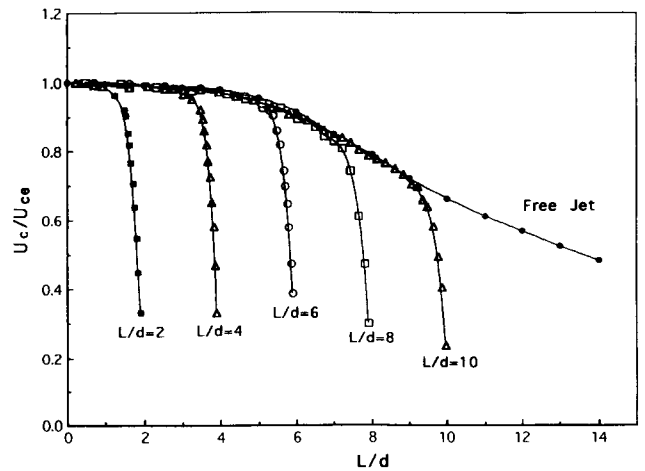

Figure 5 Free- and impinging-jet centerline velocity profiles for Re=23,000 and $d/D=0.056$

Similarly, the turbulent intensity profiles for both free jet and impinging jet (see Figure 6) remain the same down to the region corresponding to 1.3d from the surface and suddenly increase afterward, which suggests the size of impinging region. This sudden increase of the turbulent intensity and drastic decrease of the velocity on the jet centerline occurs, because high pressure created at the stagnation point due to the jet impingement obstructs the oncoming jet flow, which causes the deflection of the jet flow toward the radial direction. It has been seen from Figures 5 and 6 that deviations from the free jet flow clearly demonstrate the influence of the impinging surface on the oncoming jet flow and indicate the boundary where all impingement flow parameters have to be evaluated.

The profiles of the wall pressure coefficient along the convex surface for Re = 23,000 are shown in Figure 7. In general, C_p monotonically decreases from its maximum value at the stagnation point to zero C_p at $r/d \cong 1.5$ to negative C_p in the region corresponding to $1.5 < r/d \leq 5.5$. It is also observed that C_p at

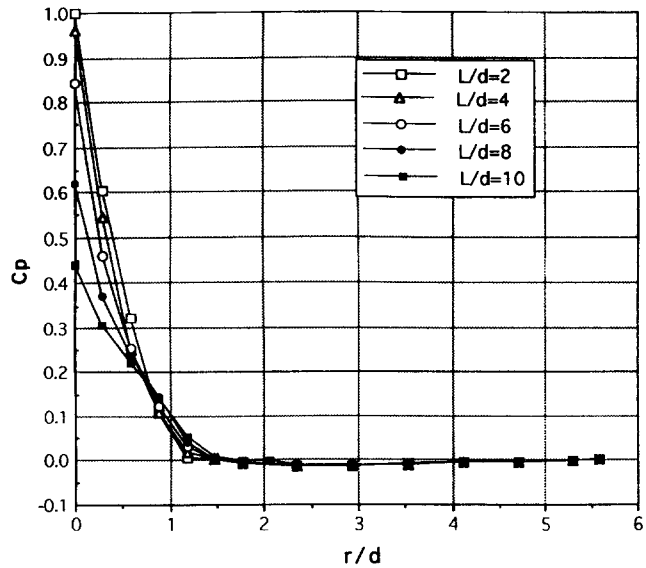

Figure 7 Profiles of the wall pressure coefficient along the convex surface for Re=23,000 and $d/D=0.056$

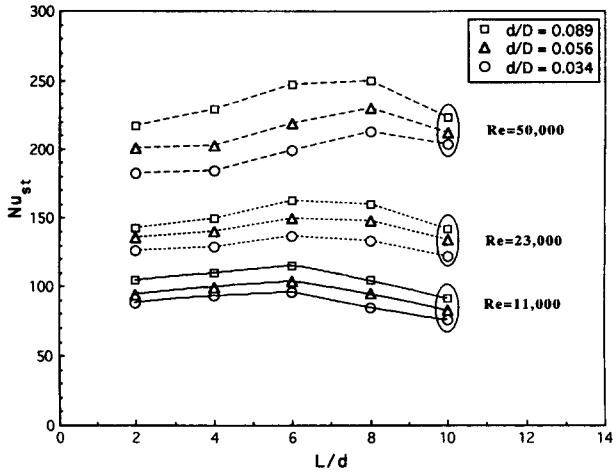

Figure 8 Effect of Reynolds number and convex surface curvature on the stagnation point Nusselt number

the stagnation point for $L/d = 4$ is as high as 96% of that for $L/d = 2$, because the impinging surface is within the potential core length for both cases according to Figure 3. For $L/d \geq 6$, C_p decreases significantly with L/d as the jet centerline velocity decays rapidly.

It is also worth noting that profiles of C_p intersect at $r/d \cong 0.77$ for all Reynolds numbers (Re = 11,000 and 50,000 cases are not shown here because of a limited space) tested. According to Rajaratnam (1976), this intersection point of C_p may be regarded as a virtual origin of the wall jet and a violent mixing of the jet impinging on the surface may occur around the point. However, to understand the exact flow behaviour better, detailed wall jet velocity and turbulence measurements must be made in that region.

Heat transfer results

The stagnation point Nusselt number (Nu_{st}) *versus* the dimensionless nozzle-to-surface distance (L/d) is plotted in Figure 8 for various surface curvatures (d/D) and Reynolds numbers. It is observed that Nu_{st} increases with increasing surface curvature (i.e., wider jet). This is attributed to increased acceleration from the stagnation point for the higher curvature, which in turn increases the heat transfer rate. In the mean time, according to Figure 9, the surface curvature effect in the wall jet region corresponding to $r/d > 2.5$ is not as significant as in the stagnation point region. Gau and Chung (1991) who investigated the surface curvature effect on a two-dimensional slot (2-D) impinging jet heat transfer from the convex semicylindrical surface also report the Nu_{st} increases with increasing surface curvature.

It is also seem from Figure 8 that Nu_{st} gradually increases with L/d and reaches a maximum of $L/d = 6$ at Re = 11,000 and 23,000, and at $L/d = 8$ for Re = 50,000, respectively. The location of the maximum Nu_{st} shifts downstream from $L/d = 6$ to $L/d = 8$ because the potential core length increases with increasing Reynolds number as shown in Figure 3. According to Figure 3 and 4, the physical mechanism for the maximum Nu_{st} to occur at $L/d = 6 \sim 8$ is that a change in the jet centerline velocity from the initial centerline velocity is not only small, but the turbulent intensity reaches roughly a maximum value in that region. This agrees well with the results of Kataoka et al. (1987), Yan (1993), and Lee et al. (1995) for a round isothermal jet impinging upon the flat surface for $10{,}000 \leq Re \leq 50{,}000$.

Correlations of Nu_{st} in terms of Re, L/d and d/D are plotted in Figures 10 and 11 and obtained as follows:

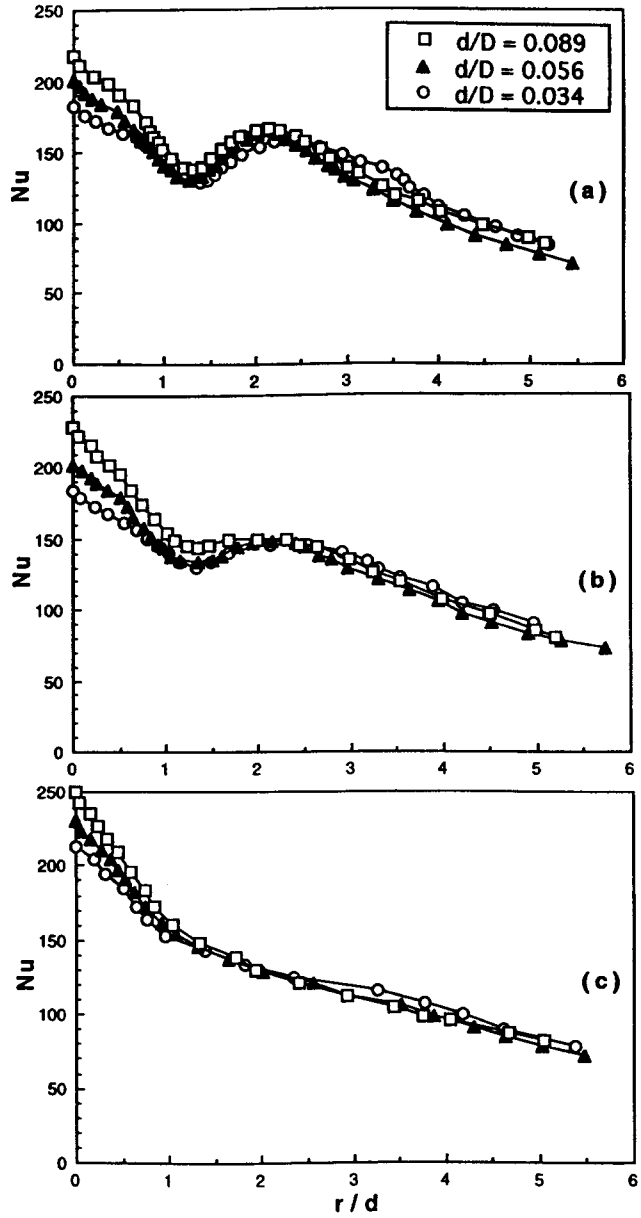

Figure 9 Effect of the convex surface curvature on the local Nusselt number for Re=50,000: (a) $L/d=2$; (b) $L/d=4$; (c) $L/d=8$

For $2 \leq L/d < 6$,

$$Nu_{st} = 1.68(Re)^{0.48}(L/d)^{0.1}(d/D)^{0.18}$$

with a scatter of 0.3%
For $6 \leq L/d \leq 10$,

$$Nu_{st} = 1.38(Re)^{0.57}(L/d)^{-0.28}(d/D)^{0.18}$$

with a scatter of 1.0%

The correlations above are valid for $11{,}000 \leq Re \leq 50{,}000$ and $0.034 \leq d/D \leq 0.089$. It should be noted that for $2 \leq L/d < 6$, Nu_{st} varies according to $Nu_{st} \propto Re^{0.48}$, which approximately agrees with the $Re^{0.5}$ laminar boundary-layer flow result and also agrees with the experimental results by Gau and Chung (1991) and Hoogendoorn (1977) for the convex surface case and flat surface case, respectively. For the longer distances, the Reynolds

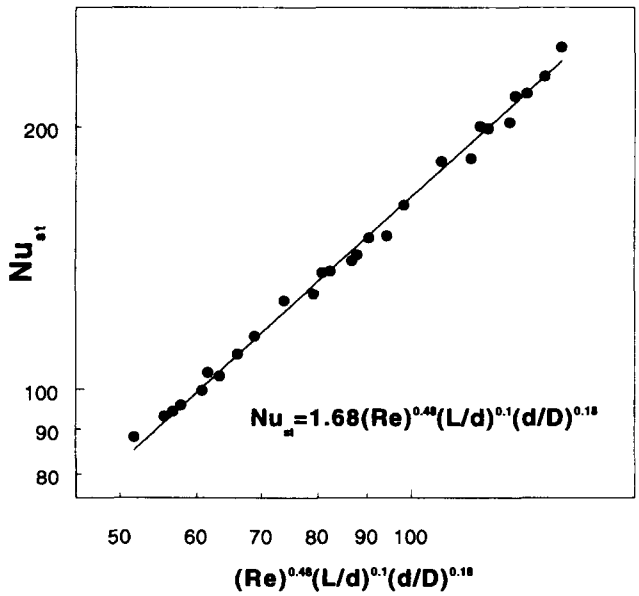

Figure 10 Correlation of the stagnation point Nusselt number on the convex surface on $2 \leq L/d < 6$

number dependence is stronger ($Nu_{st} \propto Re^{0.57}$ for $6 \leq L/d \leq 10$) due mainly to an increase of turbulence in the approaching jet as a result of the stronger exchange of momentum with surrounding ambient air. Gau and Chung also show that $Nu_{st} \propto Re^{0.5}$ for $2 \leq Z/b \leq 8$ and $Nu_{st} \propto Re^{0.54}$ for $8 \leq Z/b \leq 16$ (where, Z/b is the dimensionless nozzle-to-surface distance).

The local Nusselt number distributions along the convex surface are presented in Figures 12–15 for four nozzle-to-surface distances of $L/d = 2$, 4, 6, and 10, three jet Reynolds numbers of Re = 11,000, 23,000, and 50,000, and three nozzle-to-hemisphere diameter ratios of $d/D = 0.034$, 0.056, and 0.089. In general, the Nusselt number increases with increasing Reynolds number and surface curvature. The Nusselt number monotonically decreases from its maximum value at the stagnation point up to $r/d \cong 1.3$.

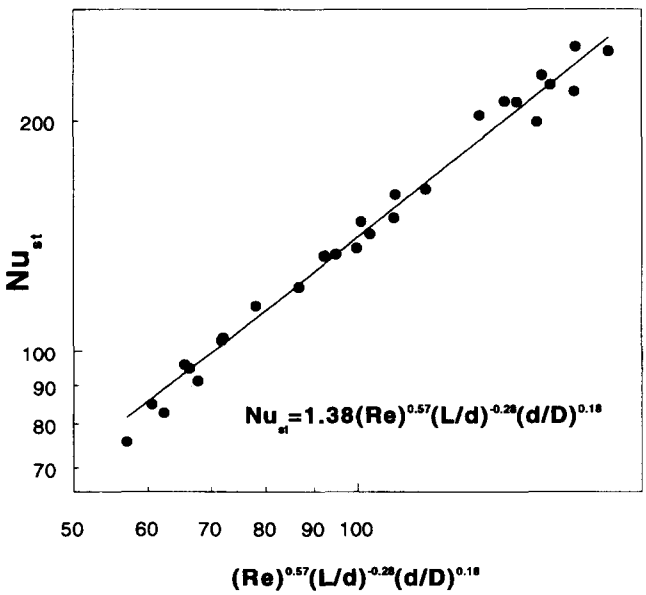

Figure 11 Correlation of the stagnation point Nusselt number on the convex surface for $6 \leq L/d \leq 10$

In general, for Re = 11,000, a gradual reduction in the Nusselt number continues (beyond $r/d \cong 1.3$) as the thermal boundary-layer thickness grows with r/d. According to Figures 12 and 13, however, for $L/d = 2$ and Re = 23,000, and for $L/d \leq 4$ and Re = 50,000, the local Nusselt number distributions exhibit increasing values in the region $1.3 \leq r/d \leq 1.5$ and attain secondary maxima at $r/d \cong 2.2$. An occurrence of the secondary maxima in the Nusselt number is attributed to the fact that when the impinging surface is within the potential core region, the potential core of the jet flow can reach the impinging surface so that the wall jet can experience a transition from laminar to turbulent flow, resulting in a sudden increase in the heat transfer rate.

When the surface is positioned outside of the potential core region (i.e., $L/d > 4$), the jet flow approaching the surface is turbulent due to a large entrainment of ambient air to the jet

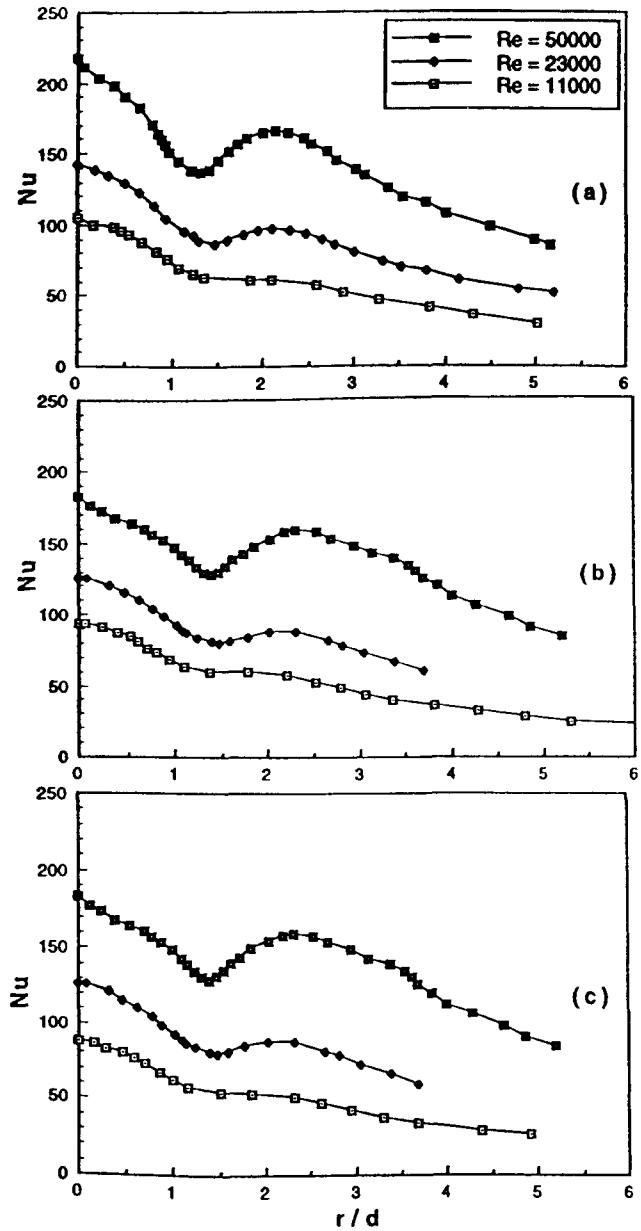

Figure 12 Streamwise distributions of the local Nusselt number for $L/D = 2$; (a) $d/D = 0.089$; (b) $d/D = 0.056$; (c) $d/D = 0.034$

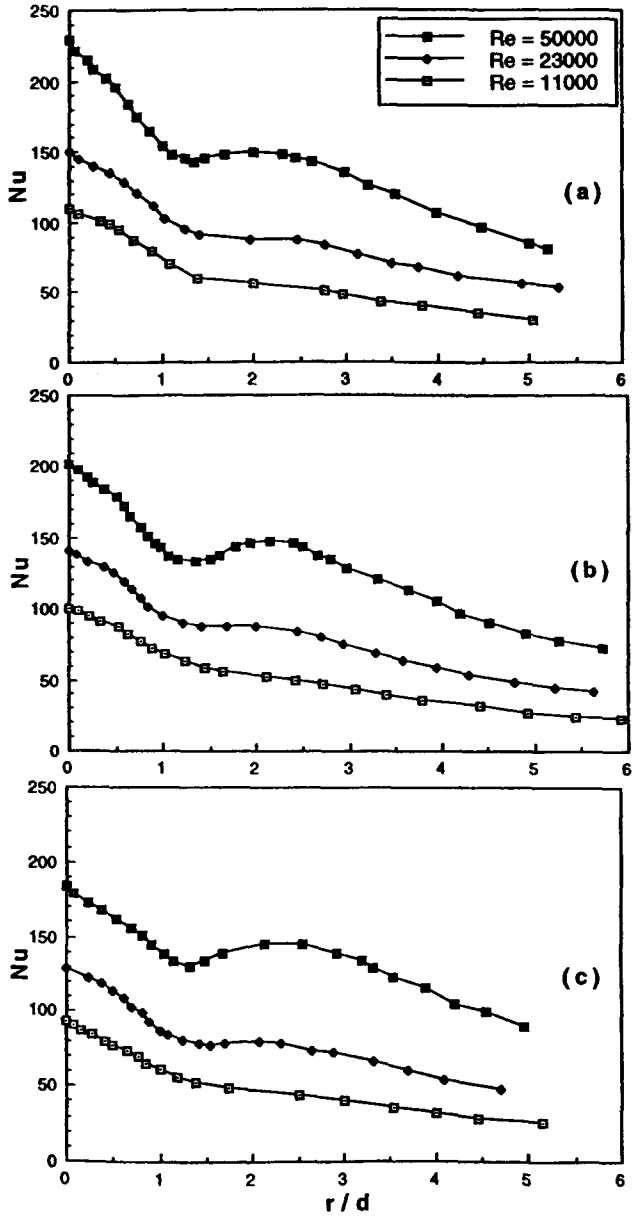

Figure 13 Streamwise distributions of the local Nusselt number for $L/d=4$: (a) $d/D=0.089$; (b) $d/D=0.056$; (c) $d/D=0.034$

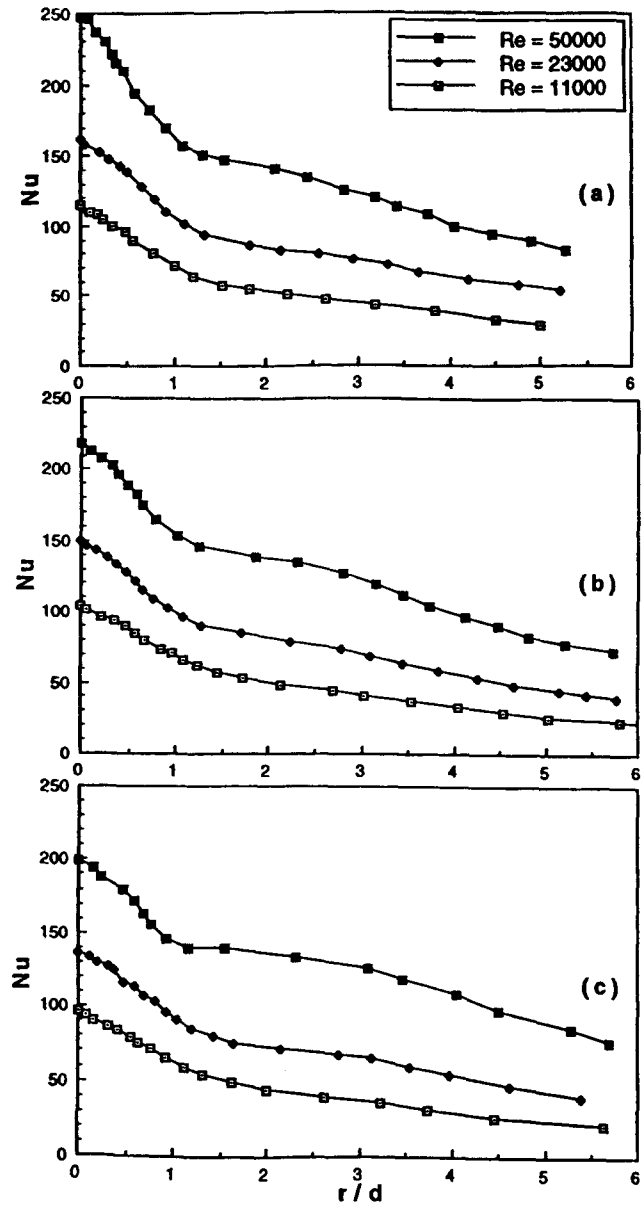

Figure 14 Streamwise distributions of the local Nusselt number for $L/d=6$: (a) $d/D=0.089$; (b) $d/D=0.056$; (c) $d/D=0.034$

flow. Therefore, a significantly higher Nusselt number at the stagnation point and a monotonic decrease of the local Nusselt number in the downstream region can be expected, as shown in Figures 14 and 15. We have previously learned from Figure 11 that for $6 \leq L/d < 10$, Nu_{st} varies according to $Nu_{st} \propto Re^{0.57}$, which is another evidence that the jet flow approaching the surface is turbulent.

The secondary maxima were also previously reported in the flat surface study by Yan (1993) and in the convex surface study by Gau and Chung (1991) at $r/d \cong 2$ for $L/d \geq 4$ and $23{,}000 \leq Re \leq 70{,}000$, and $r/b \cong 7$ for $Z/b = 4$ and $Re = 11{,}000$, respectively.

The average Nusselt number (Nu_{ave}) is obtained by integrating the local Nusselt number data over the curved surface. Nu_{ave} is also correlated with the Reynolds number, the nozzle-to-surface distance, and the nozzle-to-sphere diameter ratio for $11{,}000 \leq Re \leq 50{,}000$ and $0.034 \leq d/D \leq 0.089$.

For $2 \leq L/d < 6$,

$$Nu_{ave} = 0.6(Re)^{0.6}(L/d)^{-0.2}(d/D)^{0.38}$$

with a scatter of 1.0%

For $6 \leq L/d \leq 10$,

$$Nu_{ave} = 0.5(Re)^{0.64}(L/d)^{-0.12}(d/D)^{0.37}$$

with a scatter of 1.0%

Figures 16 and 17 present results of least-square fit to the average Nusselt number data. Similar to the stagnation point

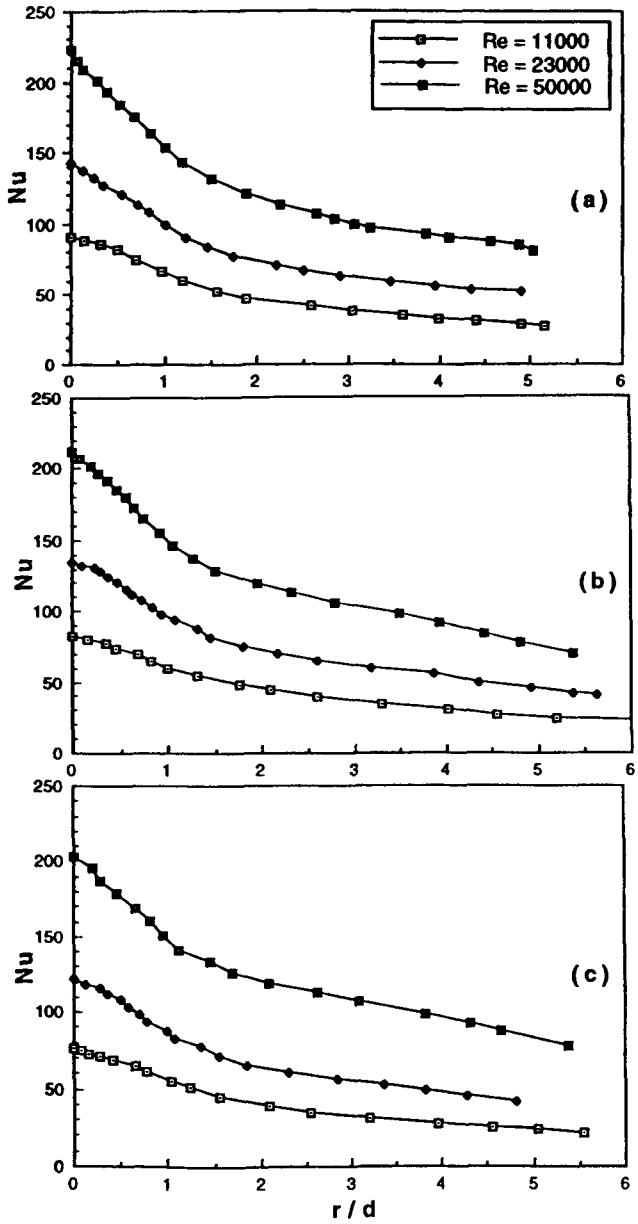

Figure 15 Streamwise distributions of the local Nusselt number for $L/d=10$: (a) $d/D=0.089$; (b) $d/D=0.056$; (c) $d/D=0.034$

Nusselt number case, for larger L/d, Nu_{ave} dependency on Re is stronger ($Nu_{ave} \propto Re^{0.64}$ for $6 \leq L/d \leq 10$, and $Nu_{ave} \propto Re^{0.6}$ for $2 \leq L/d < 6$) due to an increased momentum exchange with a surrounding air.

Conclusions

The experimental study has been carried out to investigate the effects of the hemispherically convex surface curvature on the local heat transfer of a round impinging jet issuing from a long, straight pipe nozzle. The flow results show the jet potential core extending for approximately 3.1–4.2 nozzle diameters for Re = 11,000 to 50,000. In the fully developed region corresponding to $L > 8d$, the jet centerline velocity decreases with the inverse of distance.

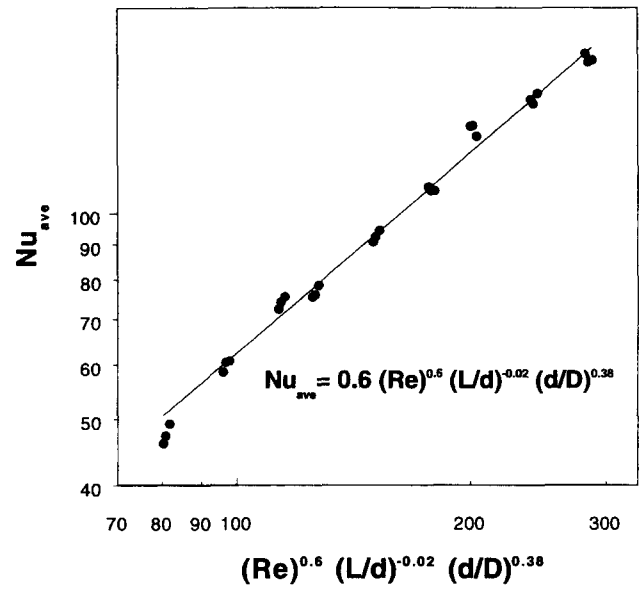

Figure 16 Correlation of the average Nusselt number on the convex surface for $2 \leq L/d < 6$

Nu_{st} increases with increasing surface curvature due to increased acceleration from the stagnation point for the higher surface curvature. At the same time, the surface curvature effect on the heat transfer is less in the wall jet region compared to the stagnation point region.

For all Res and d/D s tested, the maximum Nu_{st} occurs at $L/d \cong 6$ to 8 where a change in the jet centerline velocity from the initial velocity is not only small, but the turbulent intensity reaches roughly a maximum value in that region. The stagnation point Nusselt numbers are well correlated with Re, L/d, and d/D. For $2 \leq L/d < 6$, the correlation agrees roughly with the $Re^{0.5}$ laminar boundary-layer flow result. For the larger distances ($L/d \geq 6$), the Reynolds number dependence is stronger ($Nu_{st} \propto$

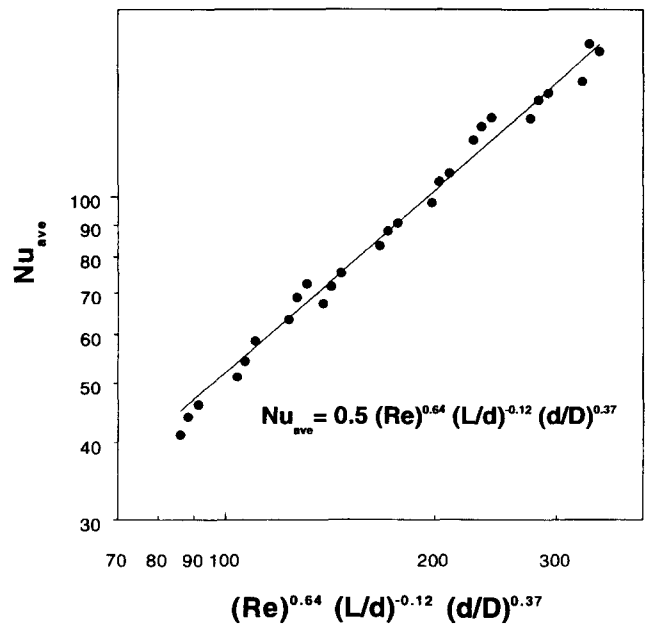

Figure 17 Correlation of the average Nusselt number on the convex surface for $6 \leq L/d \leq 10$

$Re^{0.57}$). This may be due to an increase of turbulence levels in the approaching jet flow as a result of the stronger exchange of momentum with the surrounding ambient air. The average Nusselt numbers over the curved surface are also well correlated with Re, L/d, and d/D and show a stronger dependency on Re ($Nu_{ave} \propto Re^{0.64}$ for $6 \leq L/d \leq 10$, and $Nu_{ave} \propto Re^{0.6}$ for $2 \leq L/d < 6$) for longer L/d.

The local Nusselt number decreases monotonically from its maximum value at the stagnation point. However, for $L/d = 2$ and Re = 23,000, and for $L/d \leq 4$ and Re = 50,000, the local Nusselt number distributions exhibit increasing values in the region $1.3 \leq r/d \leq 1.5$ and attain secondary maxima at $r/d \cong 2.2$. The formation of the secondary maxima is attributed to an increase in the turbulence level resulting from the transition from a laminar to a turbulent boundary layer.

Acknowledgment

This work was supported by a grant No. KOSEF 951-1007-007-1 from the Korea Science and Engineering Foundation.

References

Baughn, J. W., Ireland, P. T., Jones, T. V. and Saniei, N. 1989. A comparison of the transient and heated-coating methods for the measurements of the local heat transfer coefficients on a pin fin. *J. Heat Transfer*, **111**, 877–881

Baughn, J. W. and Shimizu, S. 1989. Heat transfer measurements from a surface with uniform heat flux and an impinging jet. *J. Heat Transfer*, **111**, 1096–1098

Boguslawski, L. and Popiel, C. O. 1979. Flow structure of the free round turbulent jet in the initial region. *J. of Fluid Mechanics*, **90**, 531–539

Chupp, R. E., Helms, H. E., McFadden, P. W. and Brown, T. R. 1969. Evaluation of internal heat transfer coefficients for impingement cooled turbine airfoils. *J. Aircraft*, **6**, 203–208

Gardon, R. and Akfirat, J. C. 1965. The role of turbulence in determining the heat transfer characteristics of impinging jets. *Int. J. Heat Mass Transfer*, **8**, 1261–1272

Gardon, R. and Akfirat, J. C. 1966. Heat transfer characteristics of impinging two-dimensional air jets. *J. Heat Transfer*, 101–108

Gardon, R. and Cobonpue, J. 1962. Heat transfer between a flat plate and jets in air impinging on it. *Int. Develop. Heat Transfer*, 454–459

Gau, C. and Chung, C. M. 1991. Surface curvature effect on slot-air jet impingement cooling flow and heat transfer process. *J. Heat Transfer*, **113**, 858–864

Giralt, F., Chia, C., and Trass, O. 1977. Characterization of the impingement region in and axisymmetric turbulent jet. *Ind. Eng. Chemistry Fundamentals*, **16**, 21–28

Goldstein, R. J. and Franchett, M. E. 1988. Heat transfer from a flat surface to an oblique impinging jet. *J. Heat Transfer*, **110**, 84–90

Hoogendoorn, C. J. 1977. The effect of turbulence on heat transfer at stagnation point. *Int. J. Heat Mass Transfer*, **20**, 1333–1338

Hrycak, P. 1981. Heat transfer from a row of impinging jets to concave cylindrical surfaces. *Int. J. Heat Mass Transfer*, **24**, 407–419

Hrycak, P. 1982. Heat transfer and flow characteristics of jet impinging on a concave hemispherical plate. *Proc. Int. Heat Transfer Conf.* **3**, 357–362

Jambunathan, K., Lai, E., Moss, M. A. and Button, B. L. 1992. A review of heat transfer data for single circular jet impingement. *Int. J. Heat and Fluid Flow*, **13**, 106–115

Kataoka, K., Sahara, R., Ase, H. and Harada, T. 1987. Role of large-scale coherent structures in impinging jet heat transfer. *J. Chem. Eng. Japan*. **20**, 71–76

Kline, S. J. and McKlintock, F. A. 1953. Describing uncertainties in single sample experiments. *Mech. Eng.* **75**, 3–8

Laufer, J. 1954. The structure of turbulence in fully developed pipe flow. NACA Rep. 1174

Lee, D. H., Greif, R., Lee, S. J. and Lee, J. H. 1995. Heat transfer from a flat plate to a fully developed axisymmetric impinging jet. *J. Heat Transfer*, **117**, 772–776

Lee, S. J., Lee, J. H. and Lee, D. H. 1994. Heat transfer measurements using liquid crystal with an elliptic jet impinging upon the flat surface. *Int. J. Heat Mass Transfer*, **37**, 967–976

Martin, H. 1977. Heat and mass transfer between impinging gas jets and solid surfaces. In *Advances in Heat Transfer*, Academic Press, San Diego, CA, **13**, 1–60

Rajaratnam, N. 1976. *Turbulent Jet*, Elsevier Scientific, The Netherlands

Thomann, H. 1968. Effect of streamwise wall curvature on heat transfer in a turbulent boundary layer. *J. Fluid Mech.* **33**, 283–292

Viskanta, R. 1993. Heat transfer to impinging isothermal gas and flame jets. *Exp. Thermal Fluid Sci.* **6**, 111–134

Yan, X. 1993. A preheated-wall transient method using liquid crystals for the measurement of heat transfer on external surfaces and in ducts. Ph.D. diss., University of California, Davis, CA

Yang, G. Y., Choi, M. S. and Lee, J. S. 1995. An experimental study of jet impinging cooling on the semi-circular concave surface. *Trans. Korea. Soc. Mech. Eng.*, **19**, 1083–1094